

Long Term study of the Schumann Resonance Regular Variations Using the Sierra Nevada station ground-based magnetometers

Alfonso Salinas¹, Jesus Rodriguez-Camacho¹, Maria C. Carrión¹, Jorge A. Portí¹, Jesús Fornieles¹, and Sergio Toledo-Redondo²

¹University of Granada

²Department of Electromagnetism and Electronics, University of Murcia

November 23, 2022

Abstract

We present a study of the Schumann Resonance (SR) regular variations (March 2013-February 2017) using the ground-based magnetometers from the Sierra Nevada station, Spain (37°02'N, 3°19'W). The study is based on the fitting parameters obtained by the Lorentzian fit, calculated for each 10-min interval record, namely, peak amplitudes, central frequencies, width of the resonances and the power spectrum integral for the first 3 SR modes. We consider three time-scales in the study: seasonal, monthly and daily variations. The processed data collected by the Sierra Nevada station are also made public with this work. The general characteristics of the long-term evolution of the Schumann resonance are confirmed, but discrepancies appear that require further study comparing recent measurements from different stations. Signatures of the influences of the El Niño phenomenon and the solar cycle to SR have been found.

1
2
3
4
5
6
7
8
9
10
11
12
13
14
15
16
17
18

Long Term study of the Schumann Resonance Regular Variations Using the Sierra Nevada station ground-based magnetometers

J.Rodríguez-Camacho¹, A. Salinas², M.C. Carrión¹, J. Portí¹, J. Fornieles-Callejón², S. Toledo-Redondo³.

¹Department of Applied Physics, University of Granada, Granada, Spain

²Department of Electromagnetism and Matter Physics, University of Granada, Granada, Spain

³Department of Electromagnetism and Electronics, University of Murcia, Murcia, Spain

Corresponding author: Alfonso Salinas (asalinas@ugr.es)

Key Points:

- Long term analysis of the Schumann resonance records at Sierra Nevada, from March 2013 to February 2017.
- The conclusions obtained partially confirm the general aspects of the long-term evolution of the Schumann resonances, but new aspects have appeared.
- Recent results on the influence of the El Niño phenomenon and the solar cycle on the Schumann resonances are confirmed.

19 Abstract

20 We present a study of the Schumann Resonance (SR) regular variations (March 2013 – February
21 2017) using the ground-based magnetometers from the Sierra Nevada station, Spain (37°02'N,
22 3°19'W). The study is based on the fitting parameters obtained by the Lorentzian fit, calculated
23 for each 10-min interval record, namely, peak amplitudes, central frequencies, width of the
24 resonances and the power spectrum integral for the first 3 SR modes. We consider three time-
25 scales in the study: seasonal, monthly and daily variations. The processed data collected by the
26 Sierra Nevada station are also made public with this work. The general characteristics of the
27 long-term evolution of the Schumann resonance are confirmed, but discrepancies appear that
28 require further study comparing recent measurements from different stations. Signatures of the
29 influences of the El Niño phenomenon and the solar cycle to SR have been found.

30 1 INTRODUCTION

31 The Schumann Resonances (SRs) are related to the propagation of the electromagnetic
32 (EM) field generated mainly by lightning events in the EM cavity delimited by the lower
33 ionosphere and the Earth's surface. This EM field belongs to the Extremely Low Frequency
34 (ELF) band of the EM spectrum, which goes from a few hertz to 50 Hz, and its spectrum shows
35 resonances at certain frequencies. This phenomenon is called SRs. In addition to the lightning
36 events produced in thunderstorms, there are some other phenomena that may contribute to the
37 SRs, like the Transient Luminous Events, TLE (Price, 2016).

38 The SR were theoretically predicted by Schumann (1952), and measured for the first time
39 by Balsler & Wagner (1960). A historical review of the SRs and of Schumann can be found in
40 Besser (2007), which shows a review of relevant works about the physical and mathematical
41 concerns of the SRs. A wide review of the theoretical bases and the experimental works aimed at
42 the study of SRs, with an emphasis on the ELF band measurement stations, can be found in
43 Nickolaenko & Hayakawa (2002). More recent works about the SRs are Simões et al. (2012),
44 Nickolaenko et al. (2016), and Price (2016). In Simões et al. (2012), the authors point out as 'one
45 of the most challenging issues identifying possible correlations between long term Schumann
46 resonance variability and climate trends. Also, the books Nickolaenko & Hayakawa (2014) and
47 Surkov & Hayakawa (2014) make up an extensive bibliographical source about the SRs and the
48 ELF field propagation in the atmosphere. The chapter about the SRs written by Sători, Mustak
49 and Williams in Betz et al. (2009) is also of great interest.

50 The research on the SRs had a resurgence at the end of the 20th century due to its relation
51 to different climate concerns. The relation between the average temperature in the tropic surface
52 and the monthly variations in the SR parameters is shown in Williams (1992). This study was
53 strengthened by Füllekrug & Fraser-Smith (1997), which linked the global lightning activity on a
54 seasonal time scale and the magnetic field variations in the lower ELF range. The SRs are a
55 useful tool to study other climatic phenomena that are influenced by the global thunderstorm
56 activity. In Sători & Zieger (1999), the variation of the global thunderstorm position southwards
57 in warm El Niño years and northwards in cool La Niña years is observed in the self-consistent
58 behaviour of the frequency level and semiannual intensity variations of the first three SR modes.
59 In a latter work, the global lightning activity on the ENSO (El Niño Southern Oscillation) time
60 scale is studied using the SRs together with data from OTD (Optical Transient Detector) and LIS
61 (Lightning Imaging Sensor) satellites in space (Sători et al., 2009). More recently, Williams et al.
62 (2021) have studied the transition between two Super-Niño periods, occurring in 1997/98 and in

63 2015/16, using data from different stations. The main conclusion is that the variations in the
64 intensity of the SRs may serve as a precursor for these extreme climate events (Williams et al.,
65 2021).

66 The solar cycle has also an impact on the SRs. In Kulak et al. (2003), it is shown that
67 when the solar activity increases the first resonant frequency also increases, and there is a small
68 decrease in the attenuation coefficient of the NS component of the horizontal magnetic field
69 measured in the East Carpathian mountains for 6 years —with some gaps in the recordings. In
70 Satori et al. (2005), data from three different ELF stations are used to confirm a rise in the
71 frequencies and in the quality factor when the solar activity increases, due to an increase in the
72 X-ray radiation. In addition to the previous results, Ondraskova et al. (2011) uses electric field
73 records to find a reduction of the differences between effective thunderstorm areas during the
74 austral and the boreal summer, and thus a prevalence of the semi-annual variations, during the
75 years of the deep solar minimum. Toledo-Redondo et al. (2012) showed a possible dependence
76 of the effective reflection height of the Earth-ionosphere cavity and the solar cycle. In
77 Nickolaenko et al. (2015), the 11-year solar cycle is analyzed using data from an ELF station in
78 Antarctica, and another ELF station located on the North Pole is added in Koloskov et al. (2020).
79 The experimental observations of these works can be explained by the point source model.

80 The importance of lightning for climate studies is increasingly recognized (Williams,
81 2005). The use of the SRs for inferring the global lightning activity achieved a broad interest, see
82 for example Nickolaenko & Rabinowicz (1995) and included bibliography. The relation between
83 the global thunderstorm activity and the diurnal first mode resonant frequency in the vertical
84 electric field component is studied in this work. This connection between the global
85 thunderstorm activity and the SRs also affects the SR amplitudes via annual and semi-annual
86 variations (Nickolaenko et al., 1998; Nickolaenko et al., 1999). A similar analysis can be found
87 in Fullekrug & Fraser-Smith (1997), where the profiling of the global thunderstorm activity is
88 made on a seasonal timescale. Another verification of the relation between the SR intensity and
89 the the global surface temperature can be found in Sekiguchi et al. (2006), where the annual and
90 semi-annual variations are also studied using Principal Component Analysis (PCA). In Belyaev
91 et al. (1999), the thunderstorms are determined making use of the Poynting vector, obtained with
92 the horizontal components of the magnetic field and the vertical component of the electric field.
93 Some advantages of the use of the Poynting vector are noted in this paper, especially when
94 records from only one station are used. This work finds a night-time peak in African
95 thunderstorm activity.

96 The thunderstorm activity in the Earth occurs mainly in three regions, located at different
97 longitudes, with a predominance of land areas. These zones are located in Central Africa and
98 Madagascar (African chimney), South and Central America, Caribbean Basin (American
99 chimney), and South-East Asia and Indonesia (Asian chimney), as shown by Christian et al.
100 (2003). These locations have their peak of activity during the local afternoon, and they largely
101 modulate the diurnal variations of the SR (e.g., Toledo-Redondo et al., 2010).

102 First studies of the long-term observations of SR can be found in Satori (1996) and Satori
103 & Zieger (1996) with data from the ELF station at the Nagycenk Observatory (47.6°N, 16,7°E),
104 Hungary. These works analyze the SR peak frequencies and amplitudes for the first three modes
105 for two years in a row. In Nickolaenko et al. (1998), records for an extra year are added to the
106 previous works and the daily frequency range variations are explored. The seasonal variations of
107 the average daily frequency pattern are also studied. A study of the long-term (4 years) diurnal,

108 seasonal and inter-annual variations in the SR parameters can be found in Price & Melnikov
109 (2004). The data are obtained from the ELF station (35.45°E, 30.35°N) near the town of Mitzpe
110 Ramon, in the Negev desert, Israel. The influence of the solar terminator passages on the SR
111 parameters in these records is addressed in Melnikov et al. (2004). In Ondrášková et al. (2007), a
112 summary of more than 4 years of continuous SR monitoring of the vertical electric component at
113 Modra Observatory (48.37°N 17.27°E) in Slovakia is presented. The monthly averaged diurnal
114 variations of the four firsts modes are analyzed. In addition, the diurnal-seasonal variations of the
115 amplitudes, frequencies and quality factors for each year are also studied. The overall pattern of
116 diurnal and seasonal variations in SR frequencies is confirmed from measurements as reported
117 from other observatory sites. In Zhou et al. (2013) and Ouyang et al. (2015), two year long
118 records from some low latitude ELF stations in China are examined. The diurnal and seasonal
119 variations in mode amplitudes and frequencies of the first four modes of SR magnetic
120 components are presented.

121 In this work, the SR regular variations obtained from the ELF station at Sierra Nevada,
122 Spain (Fornieles-Callejón et al., 2015), are analyzed from March 2013 to February 2017. This
123 ELF station records both horizontal magnetic field components, NS and EW. The processing of
124 the records is described in Rodríguez-Camacho et al. (2018). With this work the scientific
125 community is granted access to the processed data from the Sierra Nevada ELF station records.
126 The format of these data is also described in Rodríguez-Camacho et al. (2018). We consider that
127 providing the data is needed to pursue a common goal set by the SR research community, and in
128 general by the atmospheric electrodynamics research community, which is the creation of a
129 shared database of the different worldwide ELF stations. Our intention is not to set a standard for
130 the processing and the format of the data but to propose a starting point.

131 The data used in the analysis presented in this work is the output of the processing
132 scheme on the raw data, a brief explanation of this scheme is found in Rodríguez-Camacho et al.
133 (2018). Basically, each file corresponds to the amplitude spectrum of each 10 min interval and
134 the corresponding Lorentzian fitting parameters for each month in the measurement period of the
135 Sierra Nevada ELF station.

136 This paper is structured as follows: the features and structure of the Sierra Nevada ELF
137 station records are described in Section 2; the diurnal variations of the different SR parameters
138 are studied in Section 3: the seasonal variations are addressed in subsection 3.1, and the annual
139 variations from monthly averages are addressed in subsection 3.2. The time evolution of the SR
140 parameters averaging over a certain number of days, weeks or months is shown in Section 4.
141 Lastly, Section 5 corresponds to the conclusions of this work.

142

143 **2 THE SIERRA NEVADA ELF STATION RECORDS**

144 The ELF station is located in the heart of the Sierra Nevada mountains, Granada, Spain,
145 2500 m above sea level, in the area surrounding the mountain hut “Refugio del Poqueira”
146 (37°02’N, 3°19’W) (Fornieles-Callejón et al., 2015). The ELF station at Sierra Nevada is
147 equipped with two magnetometers, North-South (NS) and East-west (EW) oriented. The signal
148 detected by these magnetometers is amplified, digitized, and registered directly in the time
149 domain. The station is provided with a data acquisition system with a sampling frequency of
150 $f_s=256$ Hz. The frequency response of the magnetometers ranges from a few tenths of a hertz to

151 45 Hz. Frequencies from 6 to 25 Hz have been calibrated, thus including the first three SR
 152 modes, located around 8, 14, and 21 Hz, which are the target of the Sierra Nevada ELF station.
 153 The analog to digital converter uses 16 bit to digitize samples in the range ± 10 V. The system
 154 minimum resolution is therefore $10/2^{15} = 3.052 \times 10^{-4}$ V. Saturation limits are fixed at ± 9.990
 155 V.

156 The time domain data are processed using 10-minute long windows. For each window, the
 157 average of the amplitude spectra obtained using FFT in 10-second long intervals is calculated
 158 using the Hann window and a 5-second overlap (Welch method). A Lorentzian curve, which is
 159 the combination of three Lorentzian functions and a straight line, is fitted to the amplitude
 160 spectrum between the frequencies 6.35 Hz and 23.75 Hz, named in this paper as the fitting band.
 161 For further details of this method, see Rodríguez-Camacho et al. (2018). As a final result of the
 162 process, a file is generated for each month and sensor containing the following data:

- 163 • saturation level (ratio of saturated 10s long segments for each 10 min interval),
- 164 • amplitude spectrum for each 10 min interval,
- 165 • amplitude spectrum of the fitted signal, (the fitting curve)
- 166 • calibrated and fitting frequencies,
- 167 • fitting parameters, and
- 168 • UTC hour for the beginning of each 10 min interval.

169 The format is that generated by Numpy, a Python-based package (<http://www.numpy.org>).
 170 As explained in Rodríguez-Camacho et al. (2018), there are 11 fitting parameters in the
 171 Lorentzian fitting function: 3 individual mode amplitudes, 3 resonant frequencies, 3 half peak
 172 widths and 2 parameters corresponding to the linear part (the slope and the intercept). Once this
 173 fitting curve has been obtained, the global mode amplitudes are obtained as the value of the
 174 function at resonant frequencies. Also, from the maximum values of the fitting curve, we get the
 175 local maximum amplitudes, and the frequencies at which these maximum values appear are the
 176 local maximum frequencies. The local maximum amplitudes, together with the local maximum
 177 frequencies, will be used for the long-term analysis as they best describe the global behavior of
 178 the SRs. They will be noted as P_i (local maximum amplitudes) and fp_i (local maximum
 179 frequencies), the subindex i representing the mode ($i=1,2,3$). The integral of the power spectrum
 180 over the fitting bandwidth (6.35 - 23.75 Hz) has also been included as a parameter for the study
 181 as the power spectrum integral (PSI) of the magnetic field recorded in each sensor.

182 As commented above, the study of the regular variations of the SRs is based on the fitting
 183 parameters obtained by the Lorentzian fit, calculated for each 10-min interval records. For some
 184 intervals, the parameter values are unacceptable. This can be due to different reasons (strong
 185 lightning activity near the station, bad performance of the Lorentzian fitting algorithm, etc). For
 186 this reason, a mask is used to discard the 10-min intervals for which the values of the amplitudes

187 or the central frequencies are unacceptable. The acceptable values for the amplitudes and for the
 188 central frequencies are shown in Table 1.

189

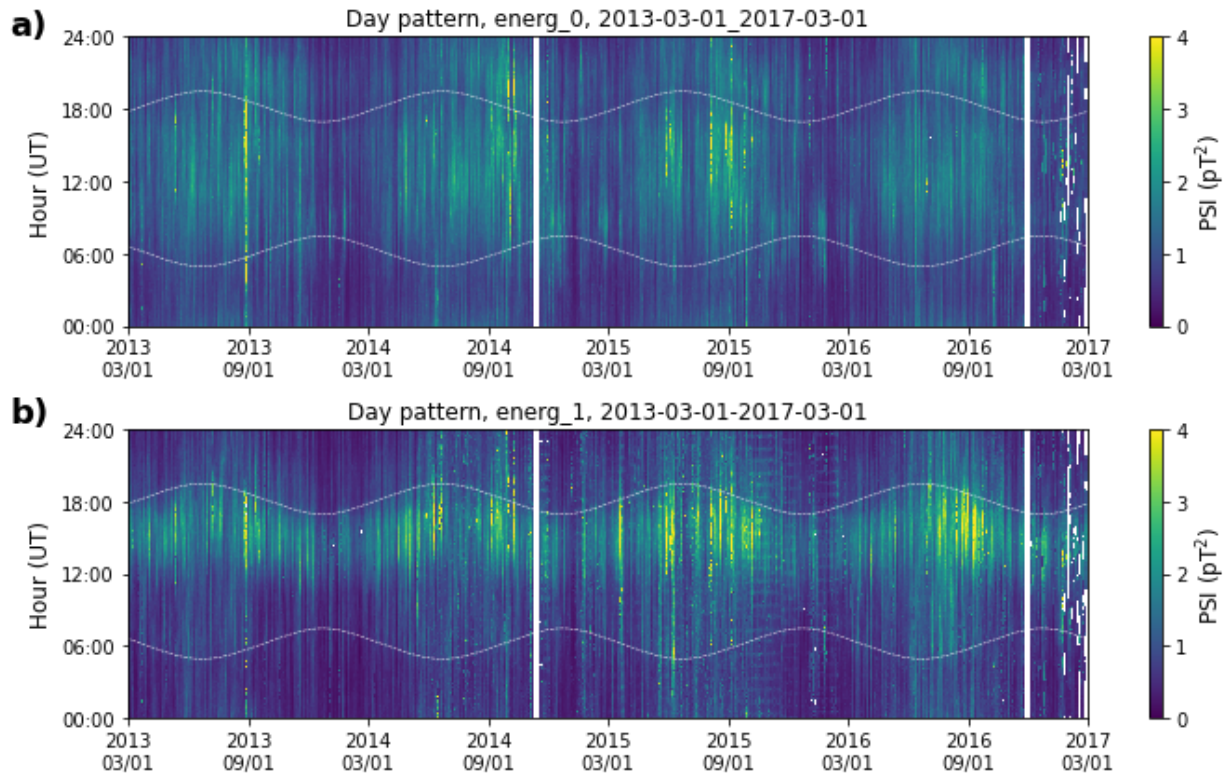
| | P_1 (pT/sqrt(Hz)) | fp_1 (Hz) | P_2 (pT/sqrt(Hz)) | fp_2 (Hz) | P_3 (pT/sqrt(Hz)) | fp_3 (Hz) |
|-------------|------------------------|-------------|------------------------|---------------|------------------------|---------------|
| Lower limit | 0.13 - 0.10 | 6.80 - 6.70 | 0.10 - 0.08 | 13.18 - 12.82 | 0.08 - 0.08 | 19.15 - 18.40 |
| Upper limit | 0.80 - 0.80 | 8.35 - 8.22 | 0.80 - 0.80 | 15.19 - 14.98 | 0.80 - 0.80 | 21.98 - 22.60 |

190 Table 1. Lowest and highest acceptable values for the local maximum amplitudes (P_1 , P_2 , P_3) and
 191 the local maximum frequencies (fp_1 , fp_2 , fp_3) for the three first modes. In each cell, the first and
 192 the second values correspond, respectively, to the NS and to the EW components.

194 In order to have a global picture of the data recorded by the Sierra Nevada ELF station,
 195 the power spectrum integral (PSI) is shown in Figure 1 for both sensors. The days are
 196 represented in the horizontal axis and the 10 min intervals of the day are represented in the
 197 vertical axis. The PSI values are shown using the colormap on the right side of the chart. The
 198 dashed white line indicates the dusk and dawn times. Vertical white lines correspond to missing
 199 data.

200

201



202

203 **Figure 1.** Power spectrum integral (PSI) for the recordings at Sierra Nevada ELF station, from
 204 03/2013 to 02/2017.

205 3 DIURNAL VARIATIONS

206 3.1 DIURNAL VARIATIONS FOR SEASONAL PERIODS

207 The local maximum amplitudes of each horizontal magnetic field component are shown
 208 in Figure 2 for each mode through a day (diurnal variations), averaged within each one of the 4
 209 astronomical seasons for the period of 4 years (from March 2013 to February 2017). A
 210 comparison of the amplitude of each magnetic field component with those shown in Zhou et al.
 211 (2013) from ELF stations located in China, the proximity of the MC thunderstorms make the
 212 amplitude in the Chinese stations be higher than in the Sierra Nevada station. The amplitude
 213 obtained in Sierra Nevada station oscillates between 0.20 and 0.45 pT/sqrt(Hz) whereas in Zhou
 214 et al. (2013) it oscillates between 0.4 and 1.2 pT/sqrt(Hz). The different thunderstorm chimneys
 215 and their impact on each component of the horizontal magnetic field can be clearly noted. It can
 216 be seen that the African thunderstorms are dominant about 1500 UT in the EW component,
 217 whereas in the NS magnetometer the thunderstorms in the Maritime Continent (MC) and
 218 America are detected with intensity peaks at 1030 and 2000 UT respectively, although the exact
 219 maximum time varies with the season.

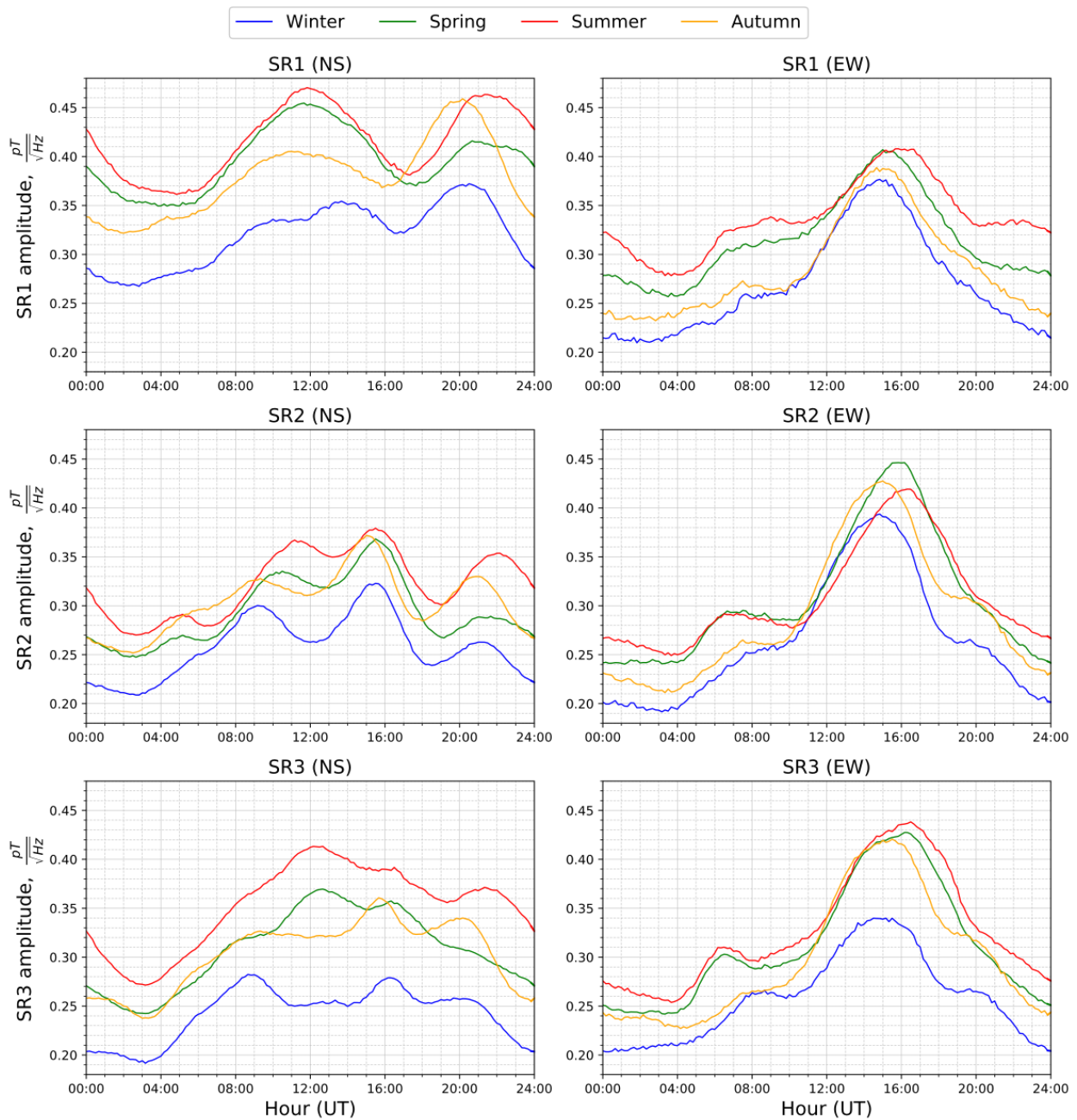
220 In the NS component the MC activity starts rising at 0400 UT and hits a maximum about
 221 1030 UT for the first mode. This maximum amplitude recorded at Sierra Nevada in this sensor

222 may be due to the superposition of the MC thunderstorms and other thunderstorms that would be
223 located at an intermediate distance, like India. Other authors, like Price & Melnikov (2004) and
224 Zhou et al. (2013), report that the maximum amplitude for the first mode about 0800 UT
225 corresponds to the MC thunderstorms but this peak does not appear in the Sierra Nevada data.
226 The reason for this may be due to the different years of the data used in the three works. For this
227 chimney, the amplitude is dominant in the summer, followed by the spring, the autumn and far
228 below the winter. This situation also occurs for the American thunderstorms, but this chimney
229 shows more activity in the autumn than in the spring. The time at which this American peak
230 happens has a strong seasonal dependence. The smallest intensity for this chimney is observed in
231 the winter, though it is the most active thunderstorm center in the winter and for the first mode
232 for all the day. In addition, throughout the day a drop in the amplitude of the 2nd and 3rd modes
233 is observed with regard to the 1st mode, and the 2nd and 3rd modes are very sensitive to the
234 African thunderstorms (between 1500 and 1600 UT).

235 For the EW component, which is more sensitive to the African thunderstorms, the
236 amplitude and shape are similar in the three modes. An amplitude peak is observed in the three
237 modes about 1500 UT and it has a stronger activity in the summer for the 1st and the 3rd modes,
238 whereas the 2nd mode is higher in the spring. A change in the time of this maximum is observed
239 when the seasons change. It goes from 1600 to 1500 UT from the summer, spring, autumn and
240 winter, and its amplitude also decreases in this order (except in the 2nd mode, for which summer
241 and spring exchange maximum amplitudes as previously noted). This peak in the summer, due to
242 the African thunderstorms, cannot be justified by the lightning observations in Blakeslee (2014),
243 where the African thunderstorms have a minimum activity in the summer. This discrepancy
244 could be due to the different years used for observation in both studies. The EW magnetometer
245 also collects a minor peak about 0600 UT, observed mainly in summer and spring, which could
246 be connected to the nighttime thunderstorms in Africa (Belyaev et al., 1999). This nighttime
247 peak is also present in Price & Melnikov (2004).

248

Seasonal variation of SR1, SR2 and SR3 global amplitudes, 2013-03-01 - 2017-03-01



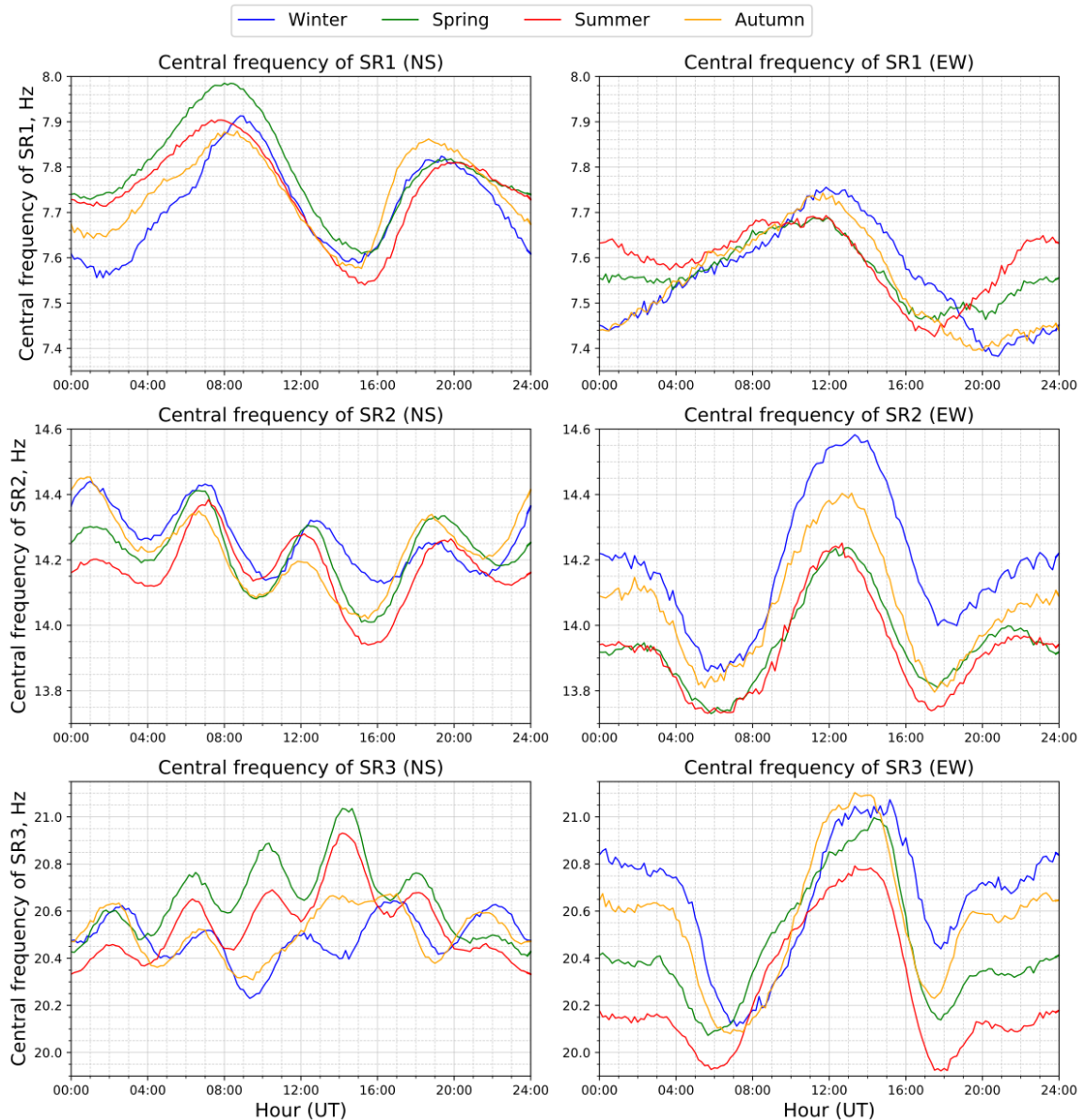
250

251 **Figure 2.** Diurnal variations of the peak amplitudes (global maximum amplitudes) for the three
 252 first modes (SR1, SR2 and SR3), in the different seasons over the recording period (2013-2017).
 253 The left column corresponds to the NS magnetometer and the right one to the EW magnetometer.
 254 Each row corresponds to a different mode (SR1, SR2 and SR3).

255 The diurnal variations of the mode central frequencies (the local maximum frequencies)
 256 for the first three modes, seasonally averaged, are shown in Figure 3. These variations of the

257 central frequencies are linked to the source-observer geometry (e.g., Toledo-Redondo et al.,
 258 2010, 2016). For both sensors, the minimum and maximum frequencies observed depend a lot on
 259 the mode, the hour of the day and the temporal definitions of the seasons themselves, as it will be
 260 shown below. In the Sierra Nevada records, unlike in other ELF stations (Price & Melnikov,
 261 2004; Zhou et al., 2013), there is not a strong seasonal dependence of the diurnal frequency
 262 variation. A transition from ‘winter-type’ to ‘summer-type’ diurnal frequency variation is not
 263 observed.

Seasonal variation of SR1, SR2 and SR3 central frequencies, 2013-03-01 - 2017-03-01



264

265 **Figure 3.** Diurnal variations of the central frequencies (global maximum frequencies) for
 266 the three first modes, in the different seasons over the recording period (2013-2017). The

267 left column corresponds to the NS magnetometer and the right one to the EW
268 magnetometer. Each row corresponds to a different mode (SR1, SR2 and SR3).

269

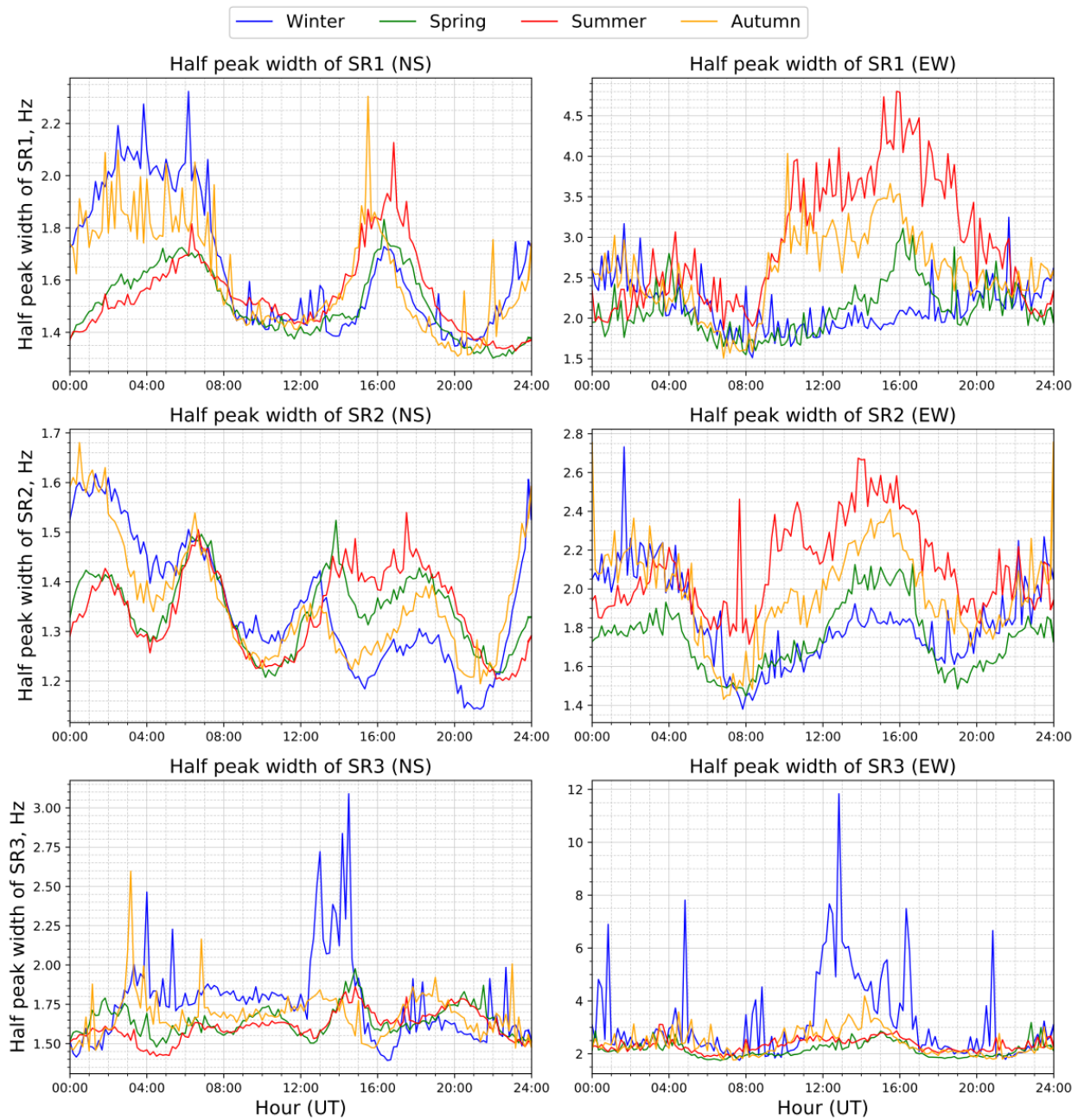
270 The analysis of the resonant peak frequency diurnal variations shows a different behavior
271 for the NS and EW components. For the NS component, the number of maxima and minima
272 observed increases by two for each mode, starting from two maxima and two minima for the first
273 mode. The first mode frequency is highest about 0800 UT and 2000 UT, and lowest about 0300
274 UT and 1500-1600 UT. These maxima and minima are also observed in the second mode at the
275 same times, together with two more maxima about 0100 UT and 1200 UT and two more minima
276 about 1000 UT and 2300 UT. In the second mode, more evident distinctions appear among the
277 different seasons, but the general pattern is still conserved. However, for the third mode there is a
278 clear distinction between the spring-summer seasons and the autumn-winter seasons. It is
279 remarkable that the third mode frequency is highest about 1400 UT in spring-summer while it
280 shows a relative minimum in winter at the same hour.

281 For the EW component the diurnal peak frequency variation for the three modes reflects a
282 rather similar pattern, with a remarkable maximum value. The highest frequency appears at 1200
283 UT, 1300 UT and 1400 UT respectively, for each mode in all season. Also, a relative maximum
284 is seen around 0000 UT that, for the first mode, is highest in the summer and it is smaller, in a
285 decreasing order, in spring, autumn and winter. For the second and third modes, the order is
286 reversed. Minimum frequencies appear about 0600-0700 UT and 1800 UT for the second and the
287 third modes, while for the first mode there is a clear lowest that occurs about 1700 UT in spring-
288 summer and about 2000 and 2100 UT in autumn and winter respectively.

289 Regarding the widths of the resonances, they show a more fluctuating behavior than the
290 other parameters. In Figure 4, it can be observed that these fluctuations do not depend much on
291 the season and they are similar for both NS and EW components. The widths are higher for the
292 EW sensor than for the NS sensor for all the modes. It is lowest in the second mode. For the third
293 mode, in the winter, several peaks are observed in the width in the EW sensor: it shows values
294 around or higher than 7 Hz, whereas it shows values between 3 and 3.5 Hz in the other seasons.

295

Seasonal variation of SR1, SR2 and SR3 widths, 2013-03-01 - 2017-03-01

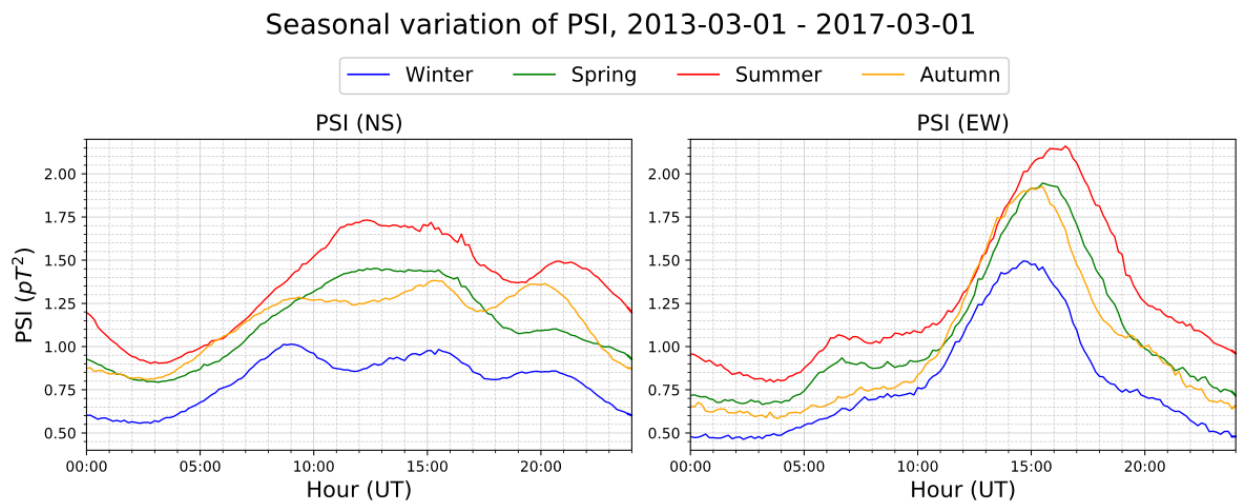


297

298 **Figure 4.** Diurnal variations of the widths of the resonances for the three first modes, in
 299 the different seasons over the recording period (2013-2017). The left column corresponds
 300 to the NS magnetometer and the right one to the EW magnetometer. Each row
 301 corresponds to a different mode (SR1, SR2 and SR3).

302 An analysis of the power spectrum integral (PSI) is shown in Figure 5 for the different
 303 seasons. This parameter is sensitive (in a nonlinear way) to the contributions of the three modes,

304 thus it can be a good indicator to be compared to the direct lightning observations from satellites,
 305 like that presented in Blakeslee et al. (2014). As in previous results, we can observe in sensor NS
 306 the activation of the thunderstorms in North America in the summer and autumn and in South
 307 America in the winter about 2100; with respect to the Asian thunderstorms (mainly observed in
 308 the NS sensor) they are maximum in the summer and the spring and we can also see the
 309 activation of Australian thunderstorms in the winter about 0800 UT. There are though some
 310 differences between the observations via satellite and those obtained from the SRs: the peak
 311 detected in the EW sensor about 0500 UT in the summer and spring (which possibly comes from
 312 African thunderstorms, as it has been commented previously) does not appear in Blakeslee et al.
 313 (2014); in the EW sensor, the African thunderstorms cause a maximum around 1600 UT in the
 314 (boreal) summer, whereas in Blakeslee et al. (2014) they show a minimum activity in the
 315 (boreal) summer.

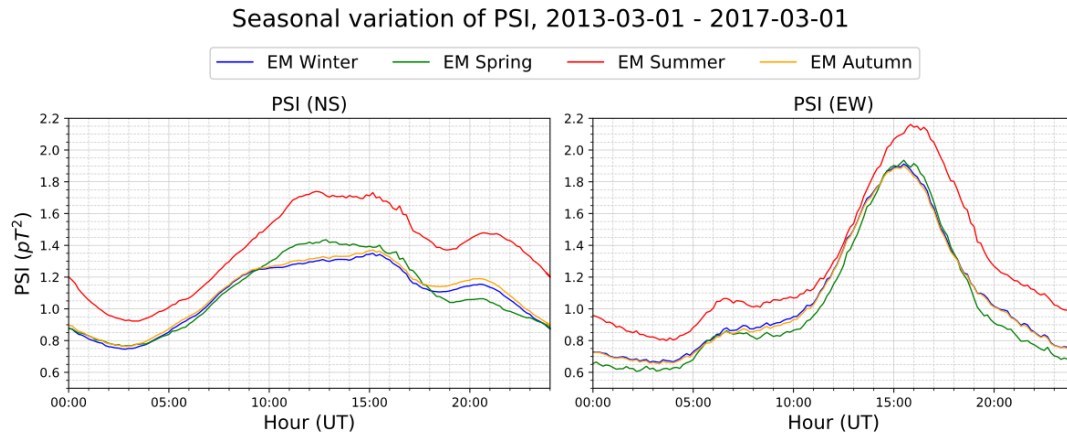


316

317 **Figure 5.** Diurnal variations of the power spectrum integral (PSI) for the different
 318 seasons over the recording period (2013-2017), in the frequency range 6.35 – 23.75 Hz.
 319 The left chart corresponds to the NS magnetometer and the right one to the EW
 320 magnetometer.

321 A definition of ‘Electromagnetic Seasons’ (EM) based on SR measurements and a
 322 numerical model is made in Nickolaenko et al. (2015). The summer is set to last from June to
 323 September, the winter is set to last from February until March, and the rest of months belong to
 324 the spring or to the autumn. The diurnal variations seasonally averaged, taking into account the
 325 setting of the seasons made by Nickolaenko et al. (2015), are shown in Figure 6 for the PSI
 326 parameter. It is interesting to compare the diurnal variations of the different parameters for both
 327 sets of seasons, the astronomical seasons in Figure 5 to the electromagnetic seasons in Figure 6.
 328 It can be noted that the seasonally averaged diurnal variations are in phase for the different

329 seasons, i.e. the maxima and minima appear at the same UT hour for all seasons. A clear
 330 difference between EM summer and the other EM seasons is also clearly shown.



331
 332 **Figure 6.** Diurnal variations of the power spectrum integral (PSI) for the different
 333 electromagnetic seasons over the recording period (2013-2017). The left chart
 334 corresponds to the NS magnetometer and the right one to the EW magnetometer.

335

336 3.2 ANNUAL DIURNAL VARIATIONS

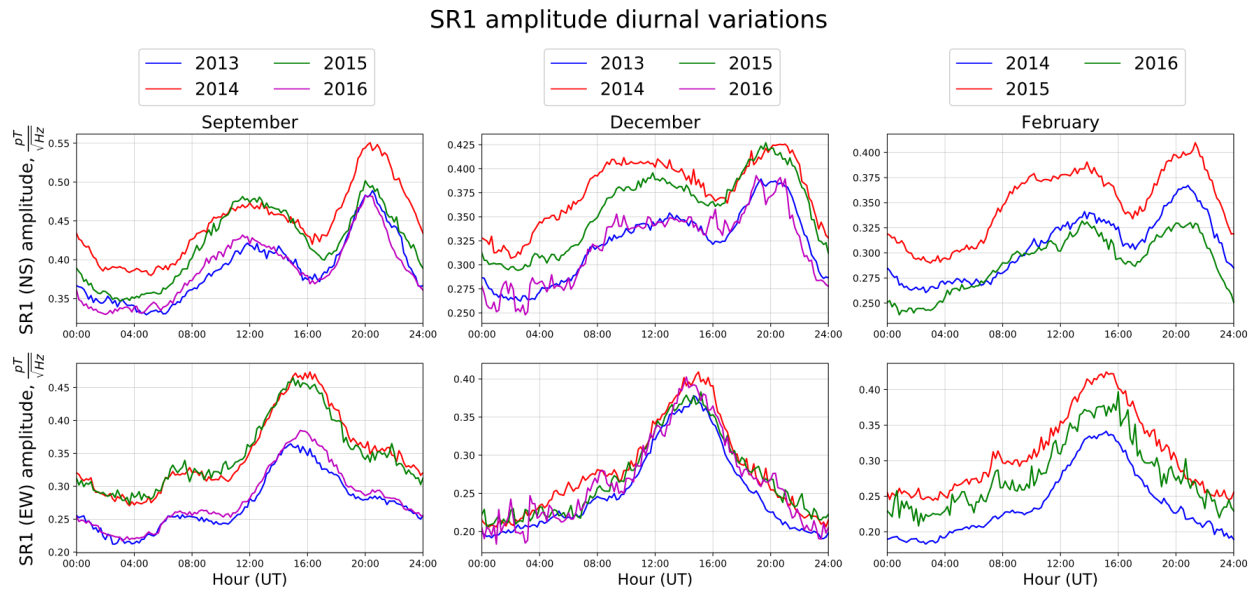
337 Another interesting indicator is the study of the diurnal variations of a parameter for a
 338 specific month over different years. The diurnal variations for the months of September,
 339 December and February are shown in Figure 7 over several years for which the recordings at the
 340 Sierra Nevada station are available. The parameter plotted is the first mode peak amplitude for
 341 each one of the horizontal components. This figure is similar to (c), (d) and (e) in figure 3 in E.
 342 Williams et al. (2021). More precisely, Figure 7 is similar to the plot of the data from
 343 Eskdalemuir station, located in a similar latitude to the Sierra Nevada station, with the only
 344 difference that the amplitude in the EW component was slightly higher in February 2016, than in
 345 2014. These results confirm the conclusions on an intensification of the SRs during the transition
 346 months that precede the super El Niño episode that happened at the end of 2015 and the
 347 beginning of 2016. We can note an intensification of the SRs in September 2014, with a
 348 maximum intensification from December 2014 to February 2015. We can also confirm a
 349 decrease in the thunderstorm activity in the declining phase of the phenomenon in February
 350 2016, though in Sierra Nevada this decrease is lower in the EW sensor than that observed in the
 351 Eskdalemuir station (Williams et al., 2021).

352 Another interesting result is related to the power spectrum integral (PSI). In Figure 8 the
 353 NS component is shown and it can be observed that two different patterns can be noted. One of
 354 them corresponds to the autumn-winter, where the three main thunderstorm centers are observed,
 355 with a predominance of the MC center in winter and American center in autumn. The other one
 356 corresponds to the summer, where African thunderstorms are dominant. However, in Figure 9,
 357 for the EW component -the most sensitive to Africa- and over the different years of recording,

358 the pattern repeats all the months with only a slight reduction in the maximum during winter
 359 months, especially in December and January.

360 In Figures 8 and 9 it can be noted that the differences among the years last for the whole
 361 day, i.e., when a parameter is higher than usual for a certain year, it is higher for every time of
 362 the day. This feature is observed in all the parameters analyzed, even those not shown in these
 363 figures. This could indicate that there is some mechanism that affects SR on a global scale.

364

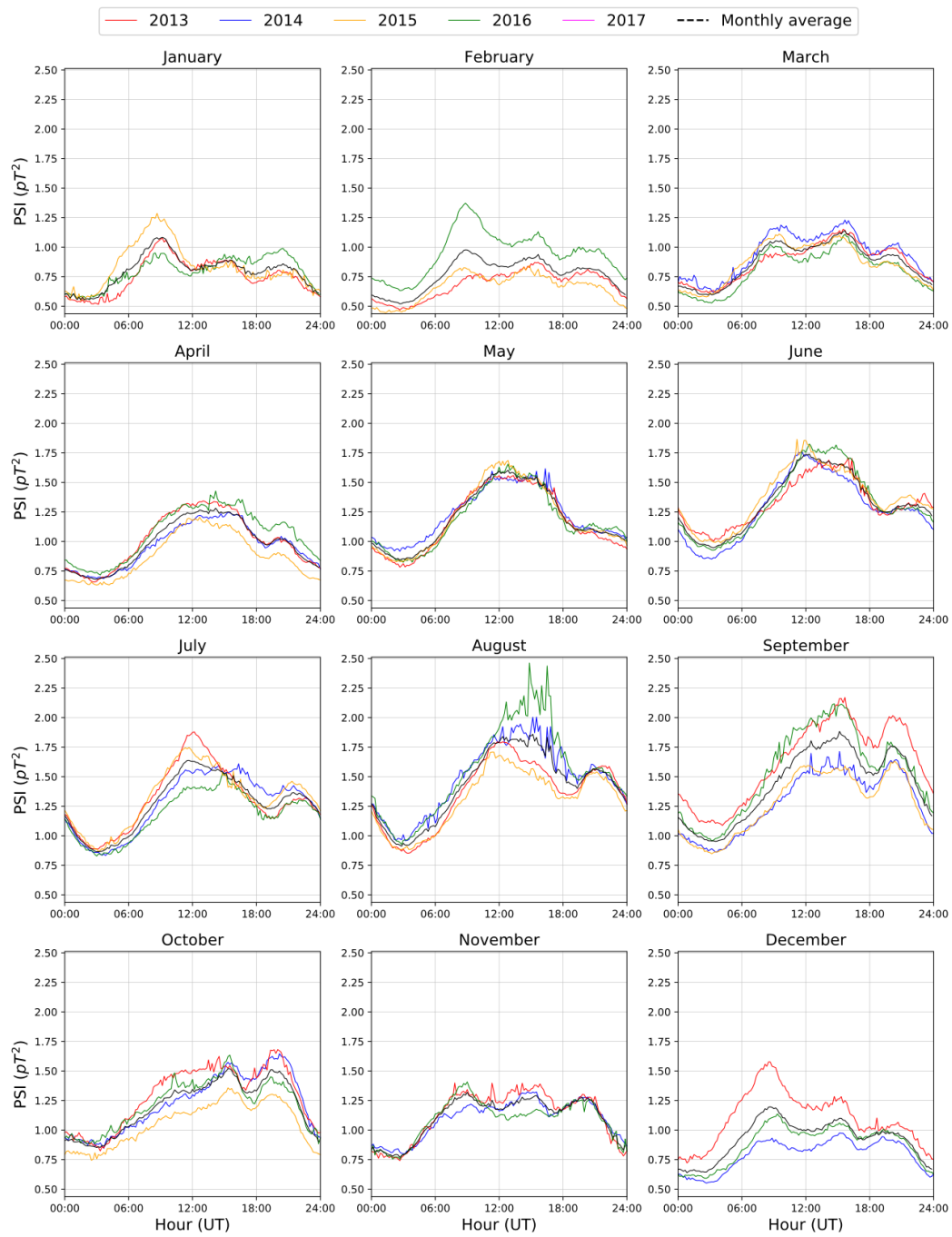


365

366 **Figure 7.** First mode peak amplitude annual diurnal variations for each one of the
 367 horizontal components for the months of September, December and February, for several
 368 years.

369

370

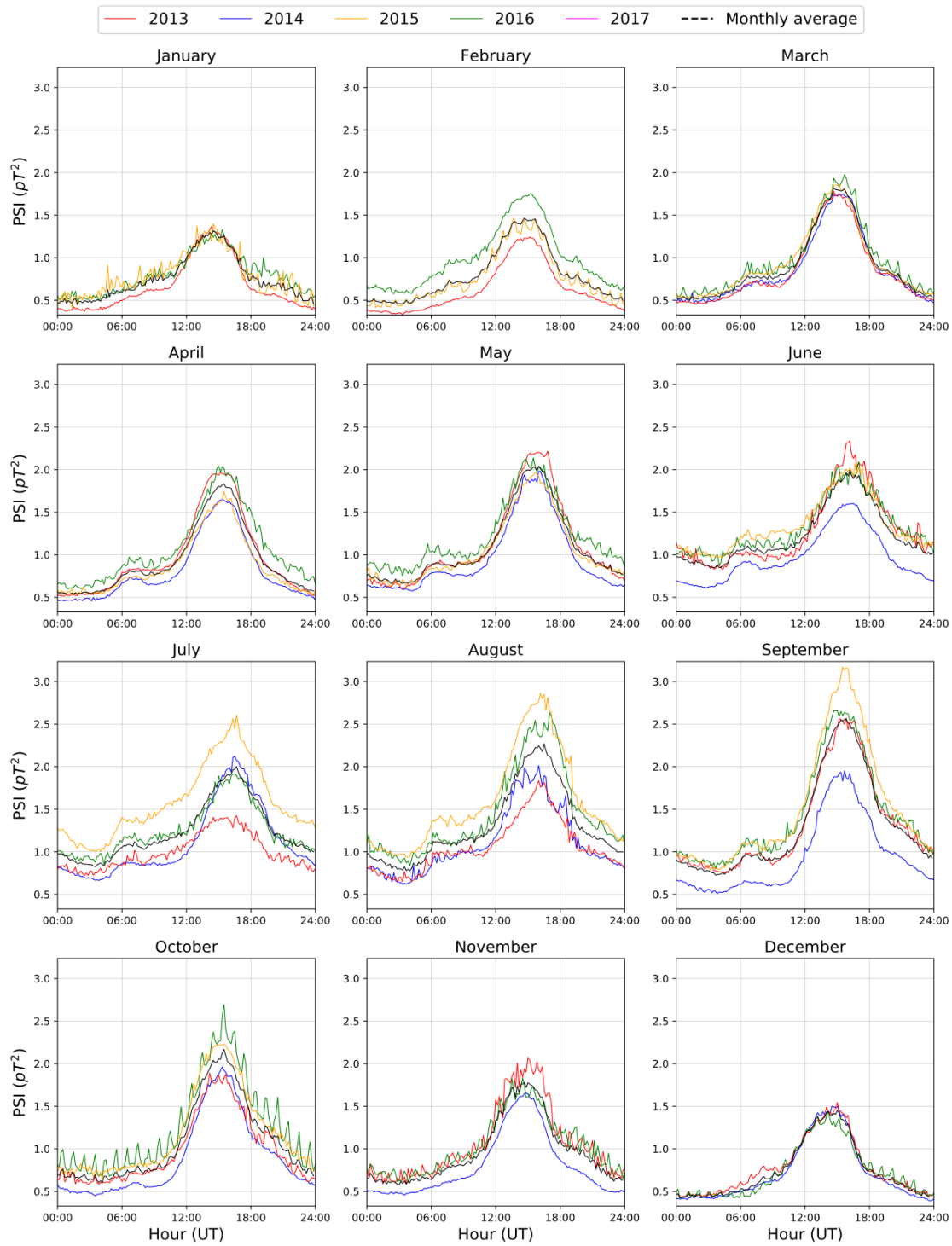


371

372

373

Figure 8. Monthly averaged diurnal variations of the power spectrum integral (PSI) during the whole recording period of the station for the NS sensors.



374

375

376

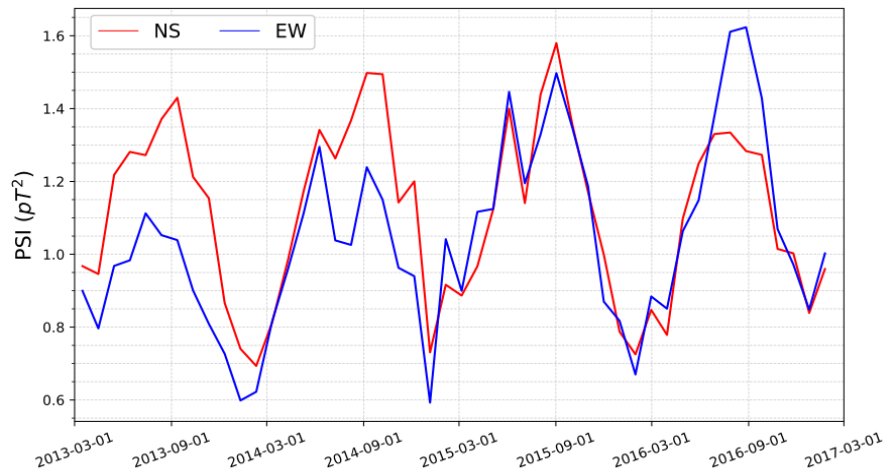
Figure 9. Monthly averaged diurnal variations of the power spectrum integral (PSI) during the whole recording period of the station for the EW sensors.

377

378 **4 DAILY VARIATIONS**

379 After studying the diurnal variations, the evolution of the parameters over the time will
 380 be addressed by averaging their values for a certain time span, which will range from 1 to 6
 381 months. In all the cases, the variation of this average is shown for the 4 years for which the
 382 records are available.

383



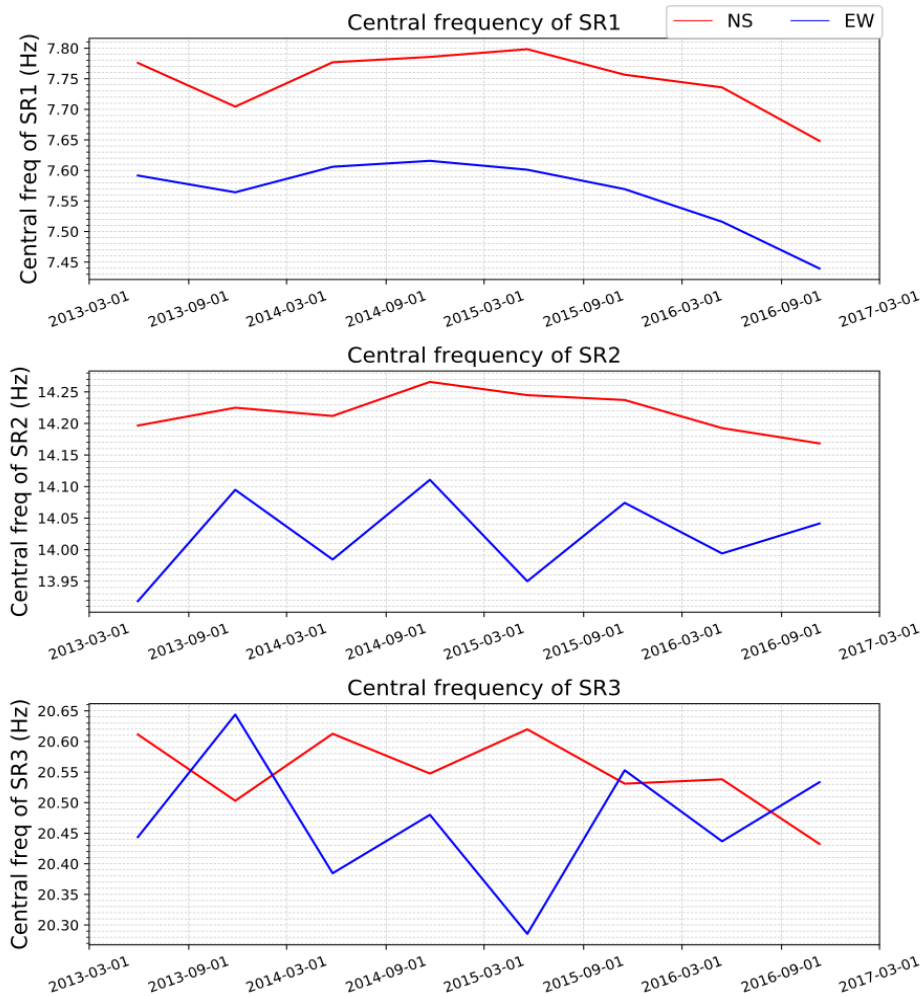
384

385 **Figure 10.** Power Spectrum Integral (PSI) averaged every 30 days, for both NS (red) and
 386 EW (blue) components.

387 The PSI for both NS and EW sensors, averaged every 30 days, is shown in Figure 10.
 388 Three clear periods can be observed. The first one goes from 2013 to the beginning of 2015,
 389 where the NS component amplitude exceeds the EW one. The second period extends over almost
 390 the whole 2015, where both components have the same amplitude. The third period begins in
 391 2016, and the EW amplitude exceeds the NS one. It is difficult to determine which
 392 thunderstorms centers are most active from the PSI observations, since the contribution of the
 393 different modes varies with each center due to the source-observer distance. But it is clear that
 394 from the end of 2014 to the beginning of 2015 there was a transition period in which the source
 395 of the SRs changed. These results agree with the ENS-ONI Index values presented in Williams
 396 et al. (2021), since this period corresponds to a transition year from the Niña period to the Super
 397 El Niño phenomenon.

398 In order to study the inter annual parameter variations and to correlate them to different
 399 phenomena in this time scale (e.g. the solar cycle), the mode peak frequency variations are
 400 shown in Figure 11 for the three modes, semi-annually averaged, to identify the referred inter
 401 annual variations. We can see some of the conclusions in Koloskov et al. (2020), connected to a
 402 tracking of the first mode resonant frequency and the 11-years cycle solar activity, during a
 403 period of large solar activity (2011 to 2017), which had a rise in 2014. The evolution of the peak
 404 frequency for the first mode presented in Figure 11, upper row, is very similar to that in figure

405 1.c in Koloskov et al. (2020), though the 24th solar cycle is not detected in the records at Sierra
 406 Nevada.

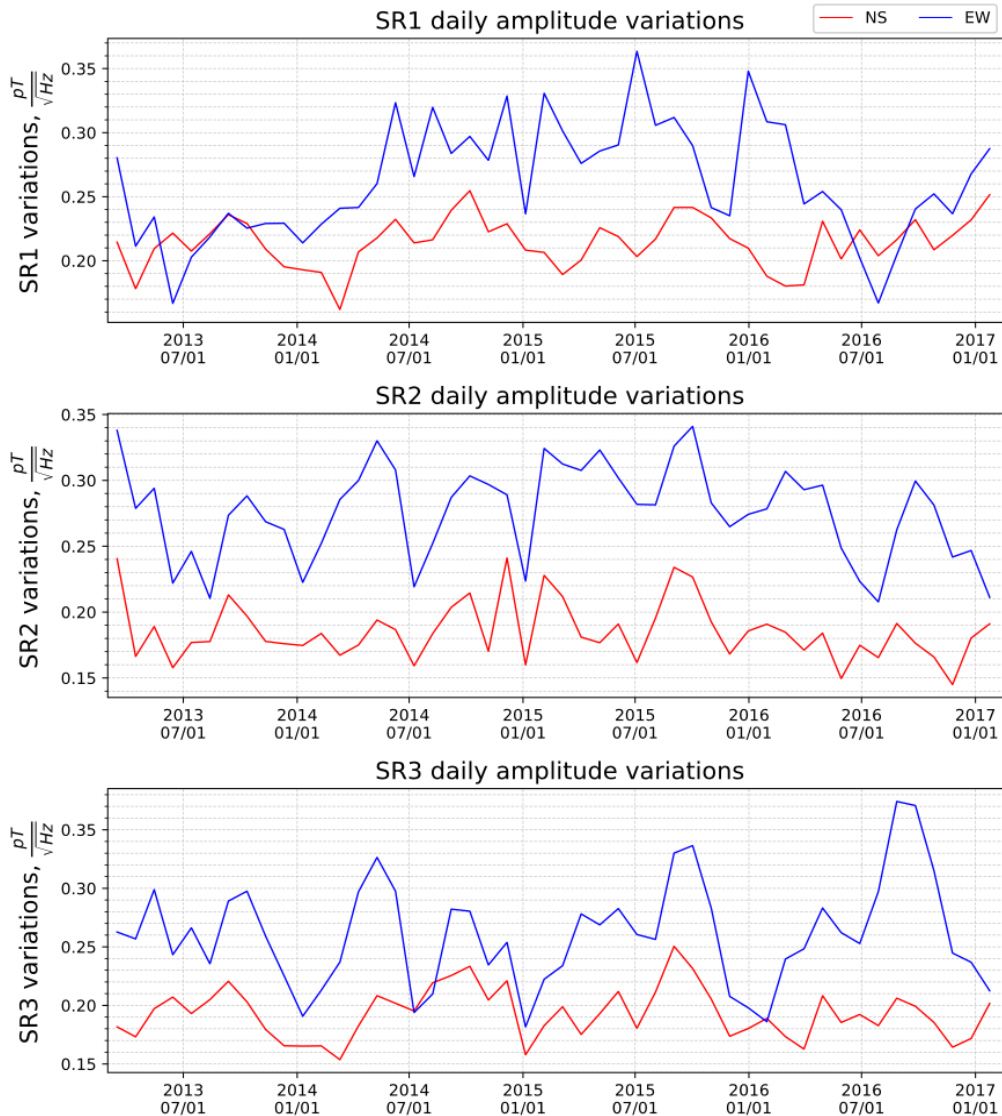


407
 408 **Figure 11.** Peak frequency daily variations averaged for a 180 days time span for both
 409 NS (red) and EW (blue) sensors. Each row corresponds to a mode, from the first to the
 410 third respectively.

411
 412 Regarding the peak frequencies for the second and third modes it can be noted, in the
 413 semi-annually averaged data, that the frequencies also tend to decrease during the years except
 414 for the sensor EW in the third mode, when a notable rise occurs in 2016, but it is soon followed

415 by a new decreasing trend. In these modes, in particular for the EW sensor, a steady semi-annual
 416 periodicity is observed in the maxima and the minima of the peak frequency.

417

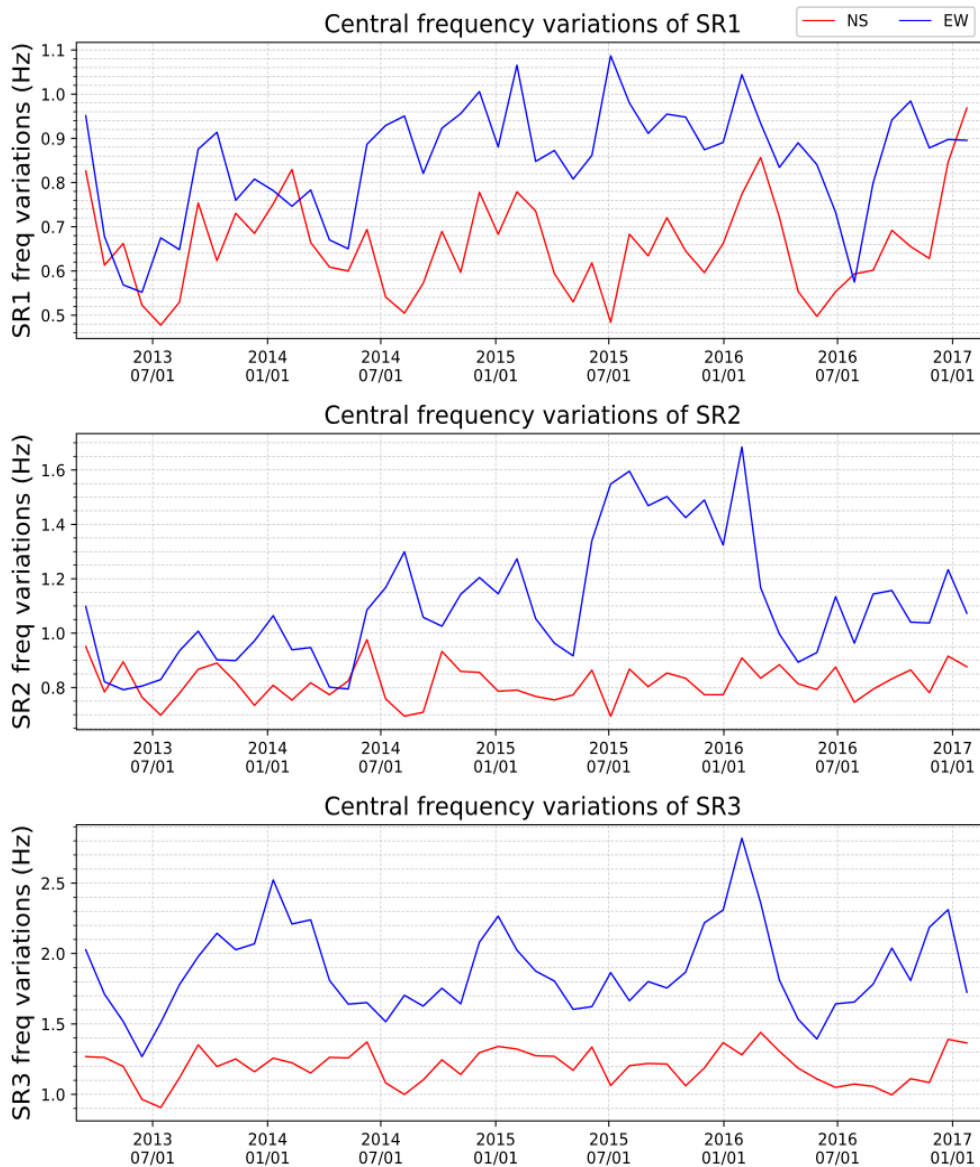


418

419 **Figure 12.** Daily variations of the peak amplitudes, averaged over 30 days, for the three
 420 first modes SR1, SR2 and SR3, in the first, the second and the third row, respectively.
 421 The NS sensor is plotted in red, and the EW sensor is in blue.

422 Another relevant concern about the time evolution of the different parameters is the
 423 minimum to maximum range of their diurnal variations. The variation of the first mode
 424 frequency for the electric field has been linked to the size of the thunderstorm center, but there is
 425 not a theoretical base on the magnetic field parameters. Figures 12 and 13 show the peak and
 426 frequency daily ranges respectively. We can see that for a 30 days average, the variations that
 427 show all the parameters in all the modes are higher for the EW sensor than for the NS sensor. In

428 the EW sensor we can clearly see an increase in the variations of the central frequency of the
 429 second mode in the year 2015. It can also be noted that no annual variations are observed in any
 430 parameter.



431

432 **Figure 13.** Daily variations of the central frequencies, averaged over 30 days, for the
 433 three first modes SR1, SR2 and SR3, in the first, the second and the third row,
 434 respectively. The NS sensor is plotted in red, and the EW sensor is in blue.

435

436

437 **5 CONCLUSIONS**

438 In this work we present a detailed analysis of the regular variations of the Schumann
439 resonances during the period March 2013 – February 2017, using Sierra Nevada station
440 (37°02'N, 3°19'W) ground-based magnetometers. Each component of the magnetic field
441 measured has been processed by fitting Lorentzian functions to the amplitude spectrum, in a
442 bandwidth of (6.35-23.75) Hz, for each 10 minutes interval of data. The regular variations of the
443 SRs have been studied using the following parameters: peak amplitudes, central frequencies, the
444 widths of the resonances and the power spectrum integral (PSI) for the three first modes. The
445 processed data for the entire measurement period of the station made public along with this
446 work, and they are presented in a Numpy npz format, which allows easy reading and subsequent
447 processing.

448 The main findings can be summarized as follows:

- 449 1. The general characteristics of the three main storm centers on Earth, Africa, CM and
450 America, in terms of their diurnal evolution have been confirmed. There is a
451 predominance of stormy activity in summer and minimal in winter. The first exhibits the
452 larger intensity and the second the longest daily duration. An additional activation time,
453 around 06:00 UT, is observed for African storm center.
- 454 2. SR2 and SR3 diurnal peak amplitudes of the NS sensor are very sensitive to the African
455 storm center. Diurnal peak amplitudes of SR1-3 in the EW sensor are similar in shape,
456 while for NS sensor the shape changes for each mode. Regarding the diurnal variation of
457 the frequency, a very different pattern is observed between the EW and NS sensors, but
458 no strong seasonal variations are observed. Sierra Nevada measurements do not exhibit a
459 transition from winter-type to summer-type variations in the diurnal variations of the
460 central frequencies. Since that parameter is related to the source-observer distance (e.g.
461 Toledo-Redondo et al., 2016), different stations are expected to exhibit different seasonal
462 patterns. The widths of the resonances are highly fluctuating and it is very difficult to
463 draw conclusions from the measurements. It is observed that the widths are greater for
464 the EW sensor than for the NS.
- 465 3. The peak amplitudes of diurnal averages measured by Sierra Nevada station are roughly
466 half of the peak amplitudes reported by the stations in China. This difference can be
467 attributed to the relative distance of each station to the storm centers. In addition, Sierra
468 Nevada station does not detect a peak in activity around 08:00 UT, that activity is shifted
469 to 10:30 UT. This may be explained by the different years considered in our study, but
470 this requires further investigation.
- 471 4. The African storm center exhibits maximums of activity during boreal summer,
472 according to our SR records. This is not well supported by global lightning data from
473 satellites (e.g., Blakeslee (2014)). A unified database involving several stations around
474 the globe would be desirable to further test these results.
- 475 5. Diurnal variations of PSI evolve with electromagnetic seasons rather than astronomical
476 seasons.

- 477 6. Predictions by Williams et al. (2021) about the effect of El Niño on SR are confirmed in
 478 our first mode peak amplitude annual diurnal variations measurements. There are also
 479 variations between EW and NS sensors: the former shows a repeating pattern every
 480 month, while the latter has different patterns during summer and winter months.
- 481 7. We find signatures in our daily variations study of the Super El Niño phenomenon during
 482 2015 and 2016, as indicated by Williams et al. (2021). We also find evidence of the solar
 483 cycle influence to SR, as in Koloskov et al. (2020).
- 484 8. Daily variations of different parameters are stronger for EW sensor than for NS sensor.

485 **Acknowledgments, Samples, and Data**

486 This work has been supported by the investigation research project FIS2017-90102-R, of the
 487 Ministry of Economy and Competitiveness (MINECO) cofinanced by the Fund European
 488 Regional Development (FEDER), and the Ministry of Education, Science and Sport of Spain
 489 through the FPU grants for PhD studentship (reference: FPU15/04291. We are grateful to Parque
 490 Nacional Sierra Nevada for providing support to the project. The data set of this paper will be
 491 available from <http://hdl.handle.net/XXXX> (At the moment we do not have a public repository
 492 for the data. Reviewers can access them (using Filezilla for example) through the server:
 493 sftp://balanis.ugr.es ; user: reviewers ; password: schumann2021 and port: 22.
 494

495 **References**

- 496
- 497 Balsler, M., & Wagner, C. A. (1960). Observations of Earth-ionosphere cavity resonances.
 498 *Nature*, *188*, 638-641. <https://doi.org/10.1038/188638a0>
- 499 Belyaev, G. G., Schekotov, A. Y., Shvets, A. V., & Nickolaenko, A. P. (1999). Schumann
 500 resonances observed using Poynting vector spectra. *Journal of Atmospheric and Solar-*
 501 *Terrestrial Physics*, *61*(10), 751-763. [https://doi.org/10.1016/S1364-6826\(99\)00027-9](https://doi.org/10.1016/S1364-6826(99)00027-9)
- 502 Besser, B. P. (2007). Synopsis of the historical development of Schumann resonances. *Radio*
 503 *Science*, *42*(2), RS2S02. <https://doi.org/10.1029/2006RS003495>
- 504 Betz, H. D., Schumann, U., & Laroche, P. (Eds.). (2009). *Lightning: Principles, Instruments and*
 505 *Applications: Review of Modern Lightning Research*. Springer Netherlands.
 506 <https://doi.org/10.1007/978-1-4020-9079-0>
- 507 Blakeslee, R. J., Mach, D. M., Bateman, M. G., & Bailey, J. C. (2014). Seasonal variations in the
 508 lightning diurnal cycle and implications for the global electric circuit. *Atmospheric*
 509 *Research*, *135-136*(Supplement C), 228-243.
 510 <https://doi.org/10.1016/j.atmosres.2012.09.023>
- 511 Christian, H. J., et al., Global frequency and distribution of lightning as observed from space by
 512 the Optical Transient Detector, *J. Geophys. Res.*, *108*(D1), 4005,
 513 doi:10.1029/2002JD002347, 2003.
- 514 Fornieles-Callejón, J., Salinas, A., Toledo-Redondo, S., Portí, J., Méndez, A., Navarro, E. A.,
 515 Morente-Molinera, J. A., Soto-Aranaz, C., & Ortega-Cayuela, J. S. (2015). Extremely

- 516 low frequency band station for natural electromagnetic noise measurement. *Radio*
517 *Science*, 50, 191-201. <https://doi.org/10.1002/2014RS005567>
- 518 Füllekrug, M., & Fraser-Smith, A. C. (1997). Global lightning and climate variability inferred
519 from ELF magnetic field variations. *Geophysical Research Letters*, 24(19), 2411-2414.
520 <https://doi.org/10.1029/97GL02358>
- 521 Koloskov, A. V., Nickolaenko, A. P., Yampolsky, Y. M., Hall, C., & Budanov, O. V. (2020).
522 Variations of global thunderstorm activity derived from the long-term Schumann
523 resonance monitoring in the Antarctic and in the Arctic. *Journal of Atmospheric and*
524 *Solar-Terrestrial Physics*, 201, 105231. <https://doi.org/10.1016/j.jastp.2020.105231>
- 525 Kulak, A., Kubisz, J., Michalec, A., Zięba, S., & Nieckarz, Z. (2003). Solar variations in
526 extremely low frequency propagation parameters: 2. Observations of Schumann
527 resonances and computation of the ELF attenuation parameter. *Journal of Geophysical*
528 *Research: Space Physics*, 108(A7). <https://doi.org/10.1029/2002JA009305>
- 529 Melnikov, A., Price, C., Sători, G., & Füllekrug, M. (2004). Influence of solar terminator
530 passages on Schumann resonance parameters. *Journal of Atmospheric and Solar-*
531 *Terrestrial Physics*, 66(13), 1187-1194. <https://doi.org/10.1016/j.jastp.2004.05.014>
- 532 Nickolaenko, A. P., & Hayakawa, M. (2002). *Resonances in the Earth-Ionosphere Cavity*.
533 Kluwer Acad., Dordrecht, Netherlands.
- 534 Nickolaenko, A. P., & Hayakawa, M. (2014). *Schumann Resonance for Tyros*. Springer, Japan.
- 535 Nickolaenko, A. P., Hayakawa, M., & Hobara, Y. (1999). Long-term periodical variations in
536 global lightning activity deduced from the Schumann resonance monitoring. *J. Geophys.*
537 *Res.*, 104(D22), 27585-27591.
- 538 Nickolaenko, A. P., & Rabinowicz, L. M. (1995). Study of the annual changes of global
539 lightning distribution and frequency variations of the first Schumann resonance mode.
540 *Journal of Atmospheric and Terrestrial Physics*, 57(11), 1345-1348.
541 [https://doi.org/10.1016/0021-9169\(94\)00114-4](https://doi.org/10.1016/0021-9169(94)00114-4)
- 542 Nickolaenko, A. P., Sători, G., Zieger, B., Rabinowicz, L. M., & Kudintseva, I. G. (1998).
543 Parameters of global thunderstorm activity deduced from the long-term Schumann
544 resonance records. *Journal of Atmospheric and Solar-Terrestrial Physics*, 60(3), 387-
545 399. [https://doi.org/10.1016/S1364-6826\(97\)00121-1](https://doi.org/10.1016/S1364-6826(97)00121-1)
- 546 Nickolaenko, A. P., V, K. A., Hayakawa, M., M, Y. Y., V, B. O., & E, K. V. (2015). 11-year
547 solar cycle in Shumann resonance data as observed in Antartica. *Sun and Geosphere*,
548 10(1), 39-49.
- 549 Nickolayenko, A. P., Shvets, A., & Hayakawa, M. (2016). *Extremely Low Frequency (ELF)*
550 *Radio Wave Propagation: A review*. 2, 91.
- 551 Ondrášková, A., Kostecký, P., Ševčík, S., & Rosenberg, L. (2007). Long-term observations of
552 Schumann resonances at Modra Observatory. *Radio Science*, 42(2), RS2S09.
553 <https://doi.org/10.1029/2006RS003478>
- 554 Ondrášková, A., Ševčík, S., & Kostecký, P. (2011). Decrease of Schumann resonance
555 frequencies and changes in the effective lightning areas toward the solar cycle minimum

- 556 of 2008–2009. *Journal of Atmospheric and Solar-Terrestrial Physics*, 73(4), 534-543.
557 <https://doi.org/10.1016/j.jastp.2010.11.013>
- 558 Ouyang, X.-Y., Xiao, Z., Hao, Y.-Q., & Zhang, D.-H. (2015). Variability of Schumann
559 resonance parameters observed at low latitude stations in China. *Advances in Space*
560 *Research*, 56(7), 1389-1399. <https://doi.org/10.1016/j.asr.2015.07.006>
- 561 Price, C. (2016). ELF Electromagnetic Waves from Lightning: The Schumann Resonances.
562 *Atmosphere*, 7(9), 116. <https://doi.org/10.3390/atmos7090116>
- 563 Price, C., & Melnikov, A. (2004). Diurnal, seasonal and inter-annual variations in the Schumann
564 resonance parameters. *Journal of Atmospheric and Solar-Terrestrial Physics*, 66(13–14),
565 1179-1185. <https://doi.org/10.1016/j.jastp.2004.05.004>
- 566 Rodríguez-Camacho, J., Fornieles, J., Carrión, M. C., Portí, J. A., Toledo-Redondo, S., &
567 Salinas, A. (2018). On the Need of a Unified Methodology for Processing Schumann
568 Resonance Measurements. *Journal of Geophysical Research: Atmospheres*, 123(23),
569 13,277-13,290. <https://doi.org/10.1029/2018JD029462>
- 570 Sători, G. (1996). Monitoring schumann resonances-II. Daily and seasonal frequency variations.
571 *Journal of Atmospheric and Terrestrial Physics*, 58(13), 1483-1488.
572 [https://doi.org/10.1016/0021-9169\(95\)00146-8](https://doi.org/10.1016/0021-9169(95)00146-8)
- 573 Sători, G., Williams, E., & Lemperger, I. (2009). Variability of global lightning activity on the
574 ENSO time scale. *13th International Conference on Atmospheric Electricity ICAE 2007*,
575 91(2–4), 500-507. <https://doi.org/10.1016/j.atmosres.2008.06.014>
- 576 Sători, G., Williams, E., & Mushtak, V. (2005). Response of the Earth–ionosphere cavity
577 resonator to the 11-year solar cycle in X-radiation. *Journal of Atmospheric and Solar-*
578 *Terrestrial Physics*, 67(6), 553-562.
- 579 Sători, G., & Zieger, B. (1996). Spectral characteristics of Schumann resonances observed in
580 central Europe. *Journal of Geophysical Research: Atmospheres*, 101(D23), 29663-29669.
581 <https://doi.org/10.1029/96JD00549>
- 582 Sători, Gabriella, & Zieger, B. (1999). El Niño related meridional oscillation of global lightning
583 activity. *Geophys. Res. Lett.*, 26(10), 1365-1368.
- 584 Schumann, W. O. (1952). Über die strahlungslosen Eigenschwingungen einer leitenden Kugel die
585 von einer Luftschicht und einer Ionosphärenhle umgeben ist. *Z. Naturforsch.*, 7a, 149-154.
586 <https://doi.org/10.1515/zna-1952-0202>
- 587 Sekiguchi, M., Hayakawa, M., Nickolaenko, A. P., & Hobara, Y. (2006). Evidence on a link
588 between the intensity of Schumann resonance and global surface temperature. *Ann.*
589 *Geophys.*, 24(7), 1809-1817. <https://doi.org/10.5194/angeo-24-1809-2006>
- 590 Simões, F., Pfaff, R., Berthelier, J.-J., & Klenzing, J. (2012). A Review of Low Frequency
591 Electromagnetic Wave Phenomena Related to Tropospheric-Ionospheric Coupling
592 Mechanisms. *Space Science Reviews*, 168(1-4), 551-593. [https://doi.org/10.1007/s11214-](https://doi.org/10.1007/s11214-011-9854-0)
593 [011-9854-0](https://doi.org/10.1007/s11214-011-9854-0)
- 594 Surkov, V., & Hayakawa, M. (2014). *Ultra and Extremely Low Frequency Electromagnetic*
595 *Fields*. Springer.

- 596 Toledo-Redondo, S., A. Salinas, J. Portí, J. A. Morente, J. Fornieles, A. Méndez, J. Galindo-
597 Zaldívar, A. Pedrera, A. Ruiz-Constán, and F. Anahnah (2010), Study of Schumann
598 resonances based on magnetotelluric records from the western Mediterranean and
599 Antarctica, *J. Geophys. Res.*, 115, D22114, doi:10.1029/2010JD014316.
- 600 Toledo-Redondo, S., M. Parrot, and A. Salinas (2012), Variation of the first cut-off frequency of
601 the Earth-ionosphere waveguide observed by DEMETER, *J. Geophys. Res.*, 117,
602 A04321, doi:10.1029/2011JA017400.
- 603 Toledo-Redondo, S., A. Salinas, J. Fornieles, J. Portí, and H. I. M. Lichtenegger (2016), Full 3-D
604 TLM simulations of the Earth-ionosphere cavity: Effect of conductivity on the Schumann
605 resonances, *J. Geophys. Res. Space Physics*, 121, doi:10.1002/2015JA022083.
- 606 Williams, E., Bozóki, T., Sători, G., Price, C., Steinbach, P., Guha, A., Liu, Y., Beggan, C. D.,
607 Neska, M., Boldi, R., & Atkinson, M. (2021). Evolution of Global Lightning in the
608 Transition From Cold to Warm Phase Preceding Two Super El Niño Events. *Journal of*
609 *Geophysical Research: Atmospheres*, 126(3), e2020JD033526.
610 <https://doi.org/10.1029/2020JD033526>
- 611 Williams, Earle R. (1992). The Schumann Resonance: A global tropical thermometer. *Science*,
612 256(5060), 1184-1187. <https://doi.org/10.1126/science.256.5060.1184>
- 613 Williams, E.R. (2005). Lightning and climate: A review. *Atmospheric Research*, 76(1-4), 272-
614 287. <https://doi.org/10.1016/j.atmosres.2004.11.014>
- 615 Zhou, H., Yu, H., Cao, B., & Qiao, X. (2013). Diurnal and seasonal variations in the Schumann
616 resonance parameters observed at Chinese observatories. *Journal of Atmospheric and*
617 *Solar-Terrestrial Physics*, 98, 86-96. <https://doi.org/10.1016/j.jastp.2013.03.021>
- 618